Optimisation-driven design to explore and exploit the process–structure–property–performance linkages in digital manufacturing

Iñigo Flores Ituarte[1] · Suraj Panicker[1] · Hari P. N. Nagarajan[1] · Eric Coatanea[1] · David W. Rosen[2,3]

Abstract

An intelligent manufacturing paradigm requires material systems, manufacturing systems, and design engineering to be better connected. Surrogate models are used to couple product-design choices with manufacturing process variables and material systems, hence, to connect and capture knowledge and embed intelligence in the system. Later, optimisation-driven design provides the ability to enhance the human cognitive abilities in decision-making in complex systems. This research proposes a multidisciplinary design optimisation problem to explore and exploit the interactions between different engineering disciplines using a socket prosthetic device as a case study. The originality of this research is in the conceptualisation of a computer-aided expert system capable of exploring process–structure–property–performance linkages in digital manufacturing. Thus, trade-off exploration and optimisation are enabled of competing objectives, including prosthetic socket mass, manufacturing time, and performance-tailored socket stiffness for patient comfort. The material system is modelled by experimental characterisation—the manufacturing time by computer simulations, and the product-design subsystem is simulated using a finite element analysis (FEA) surrogate model. We used polynomial surface response-based surrogate models and a Bayesian Network for design space exploration at the embodiment design stage. Next, at detail design, a gradient descent algorithm-based optimisation exploits the results using desirability functions to isolate Pareto non-dominated solutions. This work demonstrates how advanced engineering design synthesis methods can enhance designers' cognitive ability to explore and exploit multiple disciplines concurrently and improve overall system performance, thus paving the way for the next generation of computer systems with highly intertwined material, digital design and manufacturing workflows.

✉ Iñigo Flores Ituarte
  inigo.floresituarte@tuni.fi

1 Faculty of Engineering and Natural Sciences, Tampere University, Korkeakoulunkatu 6, 33014 Tampere, Finland

2 The George W. Woodruff School of Mechanical Engineering, Georgia Institute of Technology, Atlanta, GA 30332, USA

3 Digital Manufacturing and Design Centre, Singapore University of Technology and Design, 8 Somapah Road, Singapore 487372, Singapore

Graphical abstract
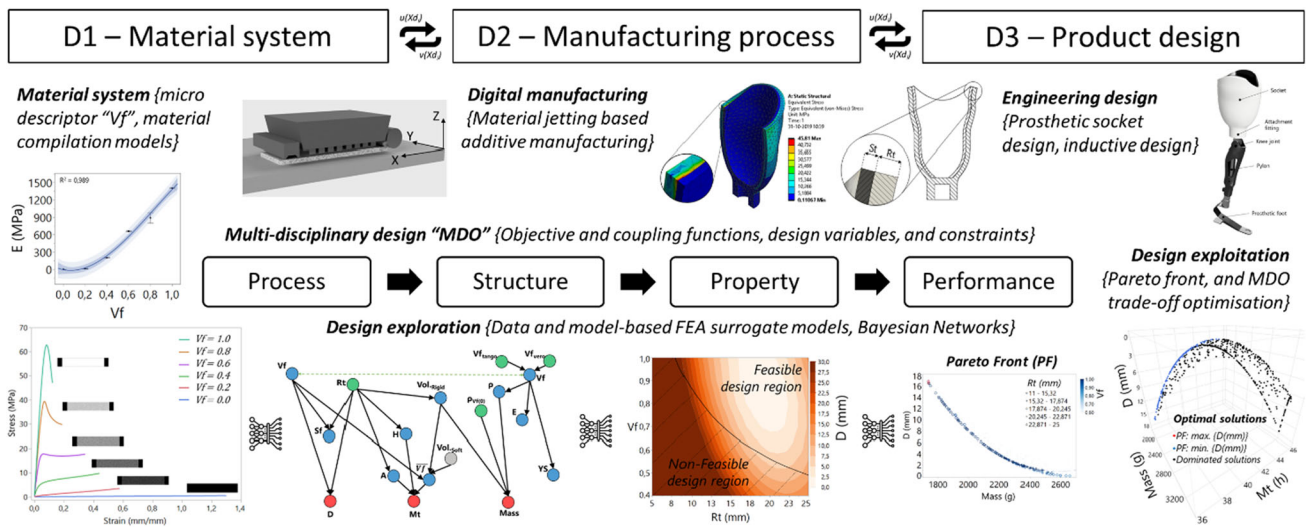
Introduction

Engineering design and manufacturing processes are a rich source of data. Data is spread across the entire product development process, including design concepts, experimental data at the material microscale, mesoscale, macroscale, simulations and test experiments, and intertwined manufacturing planning and process-related data (Oztemel & Gursev, 2020; Yan et al., 2018a, 2018b). Hypothetically, harnessing and analysing data can enable more efficient decision-making (Xiong et al., 2020). The human cognitive capabilities are limited when considering multiple complex interactions between design and performance variables, nonlinear cause-effect relationships, and large datasets that must be discovered and unveiled. Advanced design support and synthesis methods can enhance the cognitive ability of the system designer to be fully aware of the ripple effects of design choices (Nti et al., 2022). However, decision-making during engineering design is, to a large extent, conducted sequentially. The design space from product design, material selection, and manufacturing is narrowed down and optimised sequentially, without considering the complex interactions between the domains or disciplines.

The typical engineering design approach is composed of four phases, namely, (i) planning and clarification, (ii) conceptual design, (iii) embodiment design, and (iv) detail design (Pahl et al., 2007). After selecting a design concept, the objective is to explore configurations of design choices (e.g., geometrical features and material systems) that satisfy performance requirements (Xiong et al., 2019). The design space exploration at the embodiment design stage can search for potential solutions to meet design targets, defined by a set of ranges rather than specific values. On the other hand, design exploitation narrows a set of potential solutions from exploration down to one or few optimal design solutions considering design preferences. It provides ready-to-execute instructions at the detailed design stage (Xiong et al., 2020).

In a sequential product design and manufacturing process, disciplinary specialists strive to optimise objectives and satisfy constraints regarding their disciplinary variables (Hou & Jiao, 2020). The discipline-specific optimisation process can produce unintended consequences to other disciplines that prove detrimental to overall system performance. On the other hand, a concurrent engineering design approach encompasses multiple engineering disciplines simultaneously to construct a multidisciplinary design problem formulation (Balling & Sobieszczanski-Sobieski, 1996).

The primary motivation for using multidisciplinary design optimisation (MDO) is that the performance at the system level is driven not only by the performance of the individual subsystems but also by their interactions (Martins & Lambe, 2013). MDO problem formulations aim to optimise the system as a whole rather than as a collection of sequentially designed subsystems. Each disciplinary model has discipline-dependent state equations, a vector of design variables, state variables, residuals, coupling variables, functions, and constraints (Balling & Sobieszczanski-Sobieski, 1996). In MDOs, the subsystem disciplines are represented

by combining data from multi-fidelity models, including physics-based and data-driven models (aka. surrogate models) (Wang & Shan, 2006). Surrogate models represent an abstraction (i.e., an approximation or interpolation) of underlying physical phenomena (i.e., a response) over a specific region of the design space (Simpson et al., 2008), thus building the quantitative links and interdependencies between disciplines.

Intelligent manufacturing (also known as smart manufacturing) is a broad concept of manufacturing to optimise production and product transactions; therefore, interdependencies are considered between disciplines by making full use of information technologies and digital technologies for manufacturing (Zhong et al., 2017). Additive manufacturing (AM) is inherently a digital manufacturing process that enables novel methods for integrated digital design and production (Conner et al., 2014; Ballardini et al., 2018; Jiang et al., 2022). The advantage of AM technologies in product design and manufacturing is that: *"Product performance can be maximized through the synthesis of shapes, sizes, hierarchical structures and material compositions, subject to the capabilities of AM technologies"* involving a digital process from design to product (Rosen, 2014).

Olson (1997) presents materials as multilevel systems with quantitative conceptual design linkages at process, structure, property, and performance levels (PSPP). The performance of material systems rests on the twin pillars of process–structure and structure–property relations. Existing literature shows how to combine multi-physics models and data-driven methods across length scales to understand metal AM and how computational methods play a key role in understanding the fundamental PSPP relationships driving the physics and properties of AM products (Hashemi et al., 2022; Smith et al., 2016). In sum, the design freedom associated with composition and microstructure morphology and processing variables can improve products, processes and performance (Flores Ituarte et al., 2019). The process of relating properties to performance is effectively a selection-compromise exercise in which materials design becomes a multilevel and multiobjective optimisation problem (Panchal et al., 2008).

Figure 1 presents the global conceptual framework developed in this research to expand PSPP linkages to a product-level length scale while maintaining the ability to explore and exploit concurrent disciplines optimisation objectives involving quantitative linkages in digital design to manufacturing workflows. The initial hypothesis is that product design disciplinary choices can be interlinked with manufacturing processes and materials micro and mesoscale descriptors (Yan et al., 2018a, 2018b). This research conceptualises a computer-aided expert system capable of exploring process–structure–property–performance linkages to allow the trade-off optimisation of competing objectives in material, manufacturing, and product design disciplines. Hence, it contributes to enhancing the cognitive ability of system designers toward developing a new genre of multidisciplinary computational design environments (Riesenfeld et al., 2015).

The product-design discipline is represented by a prosthetic socket device exemplary case manufactured using material jetting AM. The material system disciplinary properties are modelled by experimental characterisation. The manufacturing discipline and process time are modelled by changing geometrical and material parameters in a manufacturing software pre-processor. Finally, the product-design discipline uses a prosthetic socket device as an exemplary case and is simulated using a finite element analysis surrogate model.

Limb prosthetic socket design as a case study

The use of AM and multi-material techniques in limb prosthetic design and manufacturing can enable (i) the use of a fully digital workflow to produce one-of-a-kind anatomically customized prosthetics using CT-MRI data, (ii) the use of structural optimisation to balance stiffness and lightweight design, and (iii) the combined use of multi-materials properties to create stiff and soft parts in specific zones of a one-piece socket (Comotti et al., 2017; Faustini et al., 2006; Rogers et al., 2000; Sato et al., 2016). Predominant designs such as the Patellar-Tendon Bearing (PTB) prosthesis were developed for amputee patients at the University of California at Berkeley in 1957 (Foort, 1965). This design has been regarded as the international standard for prosthetic socket devices (Hachisuka et al., 1998). By the 1980s, two new design concepts were introduced: the hydrostatic weight-bearing principle and the total surface bearing (TSB) concept (Mak et al., 2001). The basic principles for socket design vary in load distribution wherein distributing most of the load over specific load-bearing areas as in the case of PTB or more uniformly distributing the load over the entire limb as in the case of TSB design (Mak et al., 2001). Figure 2 illustrates the prosthetic socket design and exemplary results of the FEA.

As part of the research, an exemplary parametric CAD model of a TSB socket was developed. The CAD model was later used in FEA simulations performed in ANSYS mechanical. The initial dataset for the embodiment design stage is created by sampling the design space using a design of experiment (DOE), including geometrical and material variables. Figure 2a shows the complete prosthetic device, including the socket, the attachment fitting to the knee joint and pylon, and the prosthetic foot. Figure 2b shows the design of the socket, composed of two regions: (i) soft region in contact with the skin and (ii) rigid region that provides the required stiffness and structural support at the stump-socket interface.
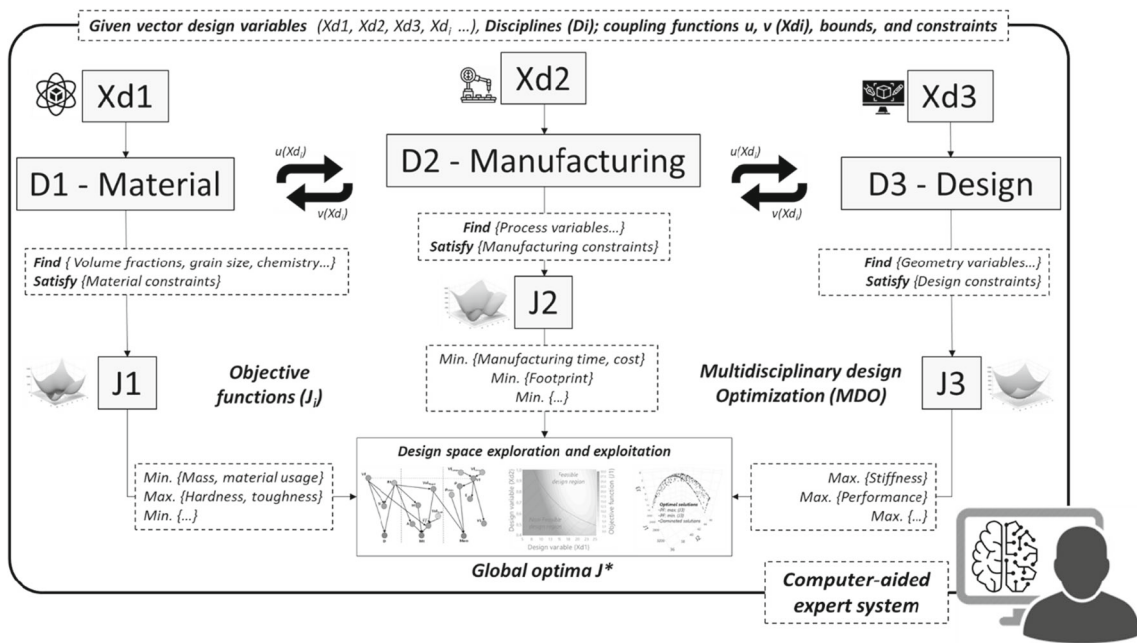
Fig. 1 Computer-aided expert system conceptual framework and methodological schema for optimization driven design of process-structure-property-performance linkages in digital manufacturing
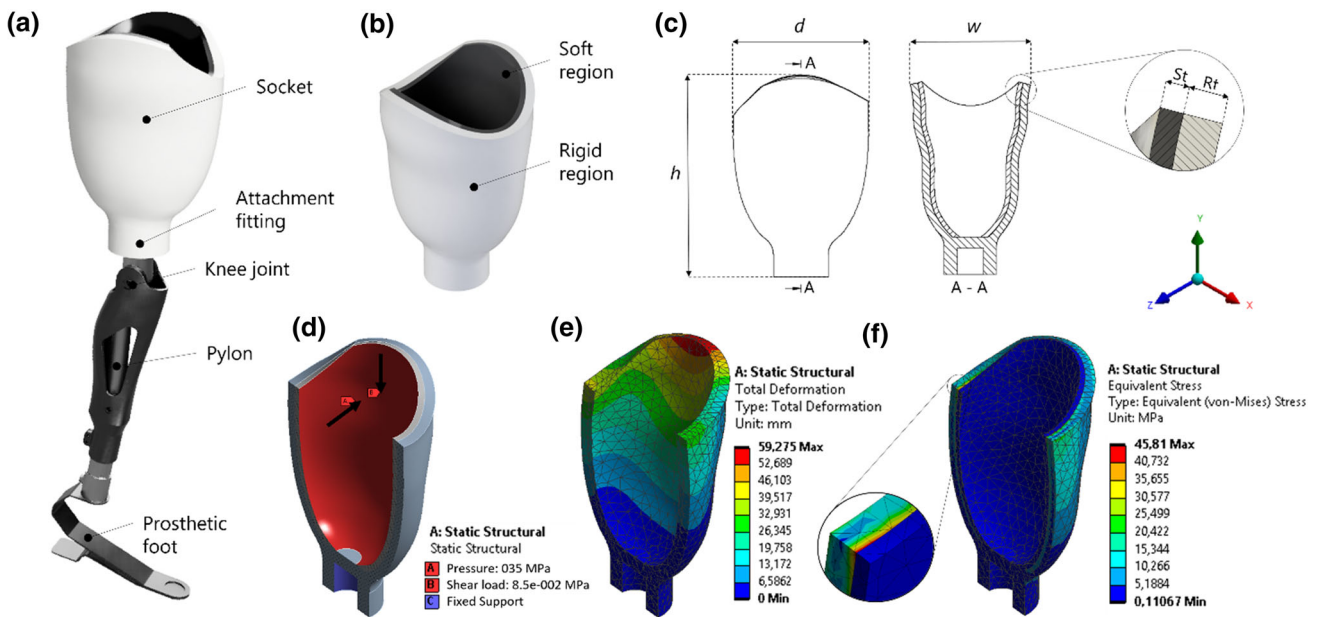

Fig. 2 Representation of the FEA model of the limb prosthetic socket product design made by AM

In this product-design exploration, the mechanical properties and thickness of the rigid region (Rt) are varied to characterize their impact on the overall volume of the socket and the resulting variation in the mass, overall stiffness of the socket and manufacturing time. Figure 2c shows the geometrical detail of the socket, with varying width (w), depth (d), and height (h) dimensions as a function of soft region thickness (St) and rigid region thickness (Rt).

The literature study found that stresses at the stump-socket interface are in two directions—pressure, perpendicular to the skin surface, and shear stress, tangential to the skin surface. Both provide support at the stump-socket interface, but above a certain level and duration can induce skin breakdown. Skin responds to pressure differently than it does to shear stress as just 8 kPa of constant pressure is sufficient to

occlude blood flow that can lead to ischemia and tissue necrosis in the patient (Sanders, 2005). Therefore, controlling the socket design's overall stiffness, flexibility, and elastic deformation can be advantageous to improving patient comfort. When walking, the pressure in the stump-socket interface for an adult male is generally below 220 kPa, with a maximum shear stress of 61 kPa (Mak et al., 2001). Existing research through FEA and experimental tests define a loading condition with 350 kPa pressure and 85 kPa shear load (Laszczak et al., 2015). Other research has shown that the maximal mean peak at the stump-socket interface pressure can go up to 215.8 kPa over the patellar tendon when walking on an incline. The maximum pressure over the popliteal area is 190.6 kPa while walking downslope (Hachisuka et al., 1998).

The literature shows that pressure and shear load in an adult male is typically equal to or lower than 350 kPa and 80 kPa, respectively. This loading condition is reported at the stump–socket interface, and it is used for the FEA in this research. Figure 2d shows how the pressure is distributed uniformly and perpendicular to the inner socket surface, and shear stress is tangential to the same surface. We applied a bonded contact between the soft and the rigid region and fixed displacement in all three axes as boundary conditions at the attachment fitting between the socket and the pylon. Figure 2e and f show one of the explored combinations of variables for the socket product design and the FEA results of total deformation and equivalent stress. The maximum stress is located between the soft and rigid regions at the interface.

MDO research design

MDO framework and decomposition of disciplines

Vertical engineering design is focused on optimisation at subsystem-level, whereas a horizontal MDO problem formulation includes coupling variables and functions between disciplines (Ferguson et al., 2009). Typically, the MDO problem formulation uses one main system-level design problem integrating subsystem-level design problems for each discipline (Balling & Sobieszczanski-Sobieski, 1996). MDOs have been used widely in the mobility industry, and aerospace wherein the optimisation problem includes structures, fatigue, propulsion, aerodynamics, payload, economics, and others disciplines as subsystems (Kodiyalam & Sobieszczanski-Sobieski, 2001; Miao et al., 2020).

In MDOs, the complexity lies at the problem formulation stage. First, it is necessary to select significant disciplinary design variables with lower and upper bounds and disciplinary optimisation objectives. Second, we need to define disciplinary models at the subsystem level and possible constraints that influence performance at the subsystem and system levels (Martins & Lambe, 2013). Third, we must consider the coupling between disciplinary models by variables and functions that interact across disciplines. The mathematical formulation of an MDO problem statement can be written as:

$$
\begin{aligned}
\min_x \quad & f(x) \\
s.t. \quad & g_i(x, u(x), v(x)) \leq 0 \\
& h_i(x, u, v) = 0 \\
& x_{LB} \leq x \leq x_{UB}
\end{aligned}
\tag{1}
$$

where $f(x)$ represent the disciplinary objective function or performance function that needs to be optimized, x is the vector of design variables, x_{LB} and x_{UB} are the lower bound and upper bound of the design variable, $u(x)$ and $v(x)$ are the coupling variables, $g_i(x)$ represent the inequality constraints, and $h_i(x)$ are general equality constraints.

Once the MDO problem is formulated, heuristic solution methods lead to non-unique conflicting optimized results, allowing the system designer to explore and exploit the design space (Kodiyalam & Sobieszczanski-Sobieski, 2001; Serhat & Basdogan, 2019). During embodiment design, the outcome of an MDO does not provide a single optimal solution that is better than the others. Instead, the objective is to unveil a region in the design space composed of a set of solutions representing the "best trade-offs". Revealing the design space mathematically can also assist in refining the region of interest that lead to a set optimal solution (Meng et al., 2021).

These solutions are called "Pareto optimal," wherein it is impossible to increase one objective's fitness without decreasing the fitness in at least another objective (Coello, 1999). Isolating the Pareto Front (PF) allows the system designer to evaluate the best trade-offs between competing objectives and exploit the design space (Ghiabakloo et al., 2016). The information obtained at the embodiment design stage can be refined and reused at the detailed design stage by focusing on a narrower non-dominated and feasible design region while exploiting a concrete system-level optimal design in a point-wise solution manner (Xiong et al., 2019).

The subsystem-level disciplines were decomposed into three domains. First, the material discipline (i.e., D1) and its vector design variables (i.e., Xd1), second, the manufacturing discipline (i.e., D2) and its vector design variables (i.e., Xd2), and third, the product-design discipline (i.e., D3) and its vector design variables (i.e., Xd3). Coupling among these three disciplines was modelled by shared functions, constraints, and variables (i.e., Di–Dj). Each discipline has its objective function (i.e., J1, J2, and J3).

When competing objective functions exist, the optimum is no longer a single design point but an entire set of non-dominated solutions referred to as the Pareto front (Ferguson et al., 2009). In MDOs, the Pareto dominance relationship is
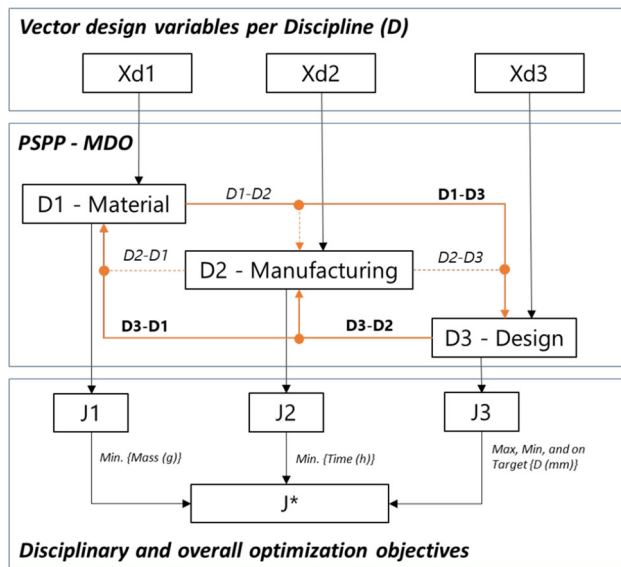
Fig. 3 Data dependence graph to decompose material discipline (D1), manufacturing discipline (D2) and product-design discipline (D3) in AM, adapted from (Martins & Lambe, 2013)

studied to distinguish the qualities of different solutions in the design space. The collection of all the Pareto optimal solutions in the decision space is called the Pareto optimal set (PS), and the projection of the PS in the objective space is called the Pareto optimal front (PF). Figure 3 shows the data dependence graph describing the MDO problem formulation. The overall optimisation objective or system-level optimisation objective (J*) is to provide feasible solutions. Thus, solutions that satisfy the imposed constraints within the given bounds isolate the Pareto Front (i.e., solutions that are non-dominated). Hypothetically, embodiment and detail design stages can utilize the MDO formulation to explore and exploit PSPP linkages while optimizing objective functions per discipline that satisfy material, manufacturing, and product-design constraints.

Material discipline

Material jetting allows combining two or more photopolymer resins that provide a range of mechanical properties from soft to rigid polymer behaviour (Mueller et al., 2015). In the process, a print block consisting of several piezoelectric inkjet heads deposits the resin droplets following predefined deposition patterns (Bass et al., 2016). Then, a roller is used to smooth each layer, and the material is

cured with an ultraviolet (UV) lamp (Ryu et al., 2019). The two photopolymers used in this work were the flexible TangoPlus (FLX980) and the rigid VeroClear (RGD810). For simplicity, we define the ratio between the two materials Vero and Tango, as volume fraction (Vf), which is defined as $Vf_{Vero} = (1 - Vf_{Tango})$. The volume fraction ($Vf$) is used as a microstructural descriptor for material homogenization which allows us to express the material behavior with simple regression models (Flores Ituarte et al., 2019). Other, variables such as infill strategies or designed hierarchical structures can affect effective mechanical properties; however, this was limited to Vf due to its statistical significance as well as to simplify the homogenization process for later FEA simulations. In sum, the regression models are used to connect the material discipline to manufacturing and product-design disciplines. Table 1 shows the design variables (Xd1) and bounds used to model the mechanical properties of the multi-material system. In this research, the material subsystem is modelled by changing the ratio of Vf from one (1) to zero (0), which implies switching between pure Vero to pure Tango.

For the characterisation of the material system, tensile specimens were fabricated in a unique build direction using the voxel printing functionality using a Stratasys J750 material jetting AM system (Stratasys). The machine was set to high-mix printing mode with a layer thickness of 0.27 mm to print the tensile specimens. The specimen's voxel size was defined as $0.42 \times 0.84 \times 0.27$ (mm), and Vf per layer of the specimen was distributed using a randomisation algorithm to obtain samples with a homogeneous material distribution. Three rectangular tensile specimens per Vf, each with a uniform Vf distribution were prepared and characterized (Flores Ituarte et al., 2019).

The dimensions for the tensile specimen were $25 \times 5 \times 60$ mm, with a cross-sectional area of 125 mm^2. The material characterisation was performed using a uniaxial tensile test on an Instron model 5982 with a 100 kN load cell and clamped with a pneumatic gripping force of approximately 10 kN. The specimens were elongated until failure at a 0.4 mm/s strain rate. Figure 4 shows the stress–strain curves obtained during the uniaxial tension tests of the tensile specimens with different Vf. Based on the tensile test, it was found that a higher Vf resulted in a stiffer material. For the tensile specimens with $Vf \geq 0.8$, the results show higher yield strength but at the cost of brittle fracture and reduced elongation capability. The specimens with $Vf \leq 0.2$ show a linear elastic

Table 1 DOE for the digital material subsystem discipline (D1)

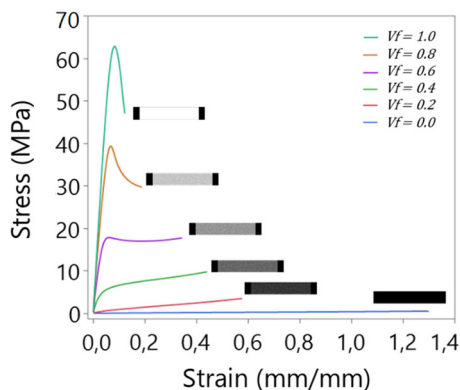| Design variable (Xd1)	Nomenclature	Levels
Volume fraction	Vf	1.0–0.8–0.6–0.4–0.2–0.0

Fig. 4 The stress–strain curves of the tested tensile specimens with a volume fraction: $0.0 \leq Vf \leq 1.0$ subject to a strain rate of 0.4 mm/s

deformation until the moment of fracture, with mechanical properties similar to rubber-like materials, such as silicone.

The tensile test results in Fig. 4 were used to build regression models for Young's modulus (E) and yield strength (YS) of the material as a function of Vf. Both regression models E and YS are used in the product-design discipline (D3) and linked to the material model subroutine in ANSYS- FEA to simulate the structural integrity of the socket.

The material subsystem optimisation objective (i.e., J1) is to minimise the mass of the obtained socket design. We found that the density of the material system changes as a function of the Vf, which influences the mass of the obtained designs. For this research, the density was modelled as a function of the Vf using the DOE reported in Table 1. The density was measured in rectangular samples with an average volume of $5.40 \pm 0.08 \text{ cm}^3$ and using a solid density analyser, Quantachrome (USA) Ultrapyc 1200e. Each sample was measured five times. The experiment data was used to build the regression models for density (ρ) as a function of Vf. Equation (2) defines the scalar form of the implemented third-order polynomial regression used to model young's modulus (E), yield strength (YS), and density (ρ) regressions as a function of Vf:

$$y = \beta_o + \sum_{i=1}^{k} \beta_i x_i + \sum_{i=1}^{k} \beta_{ii} x_i^2 + \sum_{i=1}^{k} \beta_{iii} x_i^3 + \varepsilon \quad (2)$$

where ε is the unobserved random error, β with appropriate subscript represents the coefficients of the regression model for each term (i.e. intercept β_o, first order β_i, quadratic β_{ii}, and cubic β_{iii}). These are calculated by the least-squares method. x_i represents the independent variable Vf and y corresponds to the dependent variables (i.e., E, YS, and ρ).

All first, second, and third-order terms were included in the test to construct the regression models. A stepwise regression approach was used to eliminate non-significant terms and find the most parsimonious model. The stopping rule was set with a forward P-value threshold significance to enter at P-value ≤ 0.25, which represents the maximum P-value that a term must have to be included in the model during a forward step. A detailed discussion regarding the regression results for E, YS, and ρ as a function of Vf is presented in Appendix 1. Figure 5 displays the resulting regression models for E, YS, and ρ, as a function of Vf microstructural descriptor. All three figures display the confidence interval at 95%, which represents a range of likely values for the mean response, as well as the prediction interval at 95%, which is the range of likely values for new observations. Figure 5a shows the obtained regression function for Young's modulus (E) as a function of Vf.

To simplify the regression model for E, we reduced the product-design exploration to $0.4 \leq Vf \leq 1.0$ region. The material design space shows that the variation of Vf (i.e., the ratio between Vero and Tango material) provides a range of Young's modulus values between 200 ± 1.15 MPa (i.e., $Vf = 0.4$) and 1401.67 ± 2.03 MPa (i.e., $Vf = 1$). Figure 5b shows the obtained regression function for yield strength (YS) as a function of Vf. The variation of Vf provides a yield strength range between 5.03 ± 0.08 MPa (i.e. $Vf = 0.4$) and 60.75 ± 0.38 MPa (i.e. $Vf = 1$). The optimisatin objective J1 is to minimise the mass of the socket design. The change in Vf leads to changes in the obtained material density which in turn impacts mass. Figure 5c shows the regression function for density as a function of Vf. In this case, a higher Vf result in a denser material. The results show that the variation of Vf provide a density range between 1.119 ± 0.061 g/cm^3 ($Vf = 0.0$) and 1.177 ± 0.002 g/cm^3 ($Vf = 1.0$).

Manufacturing discipline

Voxel-based multi-material jetting AM allows fabrication of materials systems at the mesoscale ($\sim$1 mm) by controlling the deposition patterns of soft elastomeric and rigid glassy polymers at the voxel-scale ($\sim$90 μm) in a layer by layer approach (Flores Ituarte et al., 2019). The most significant factor that determines the manufacturing time (Mt) in AM is often related to the vertical height of the part due to the part orientation effect on the layer by layer manufacturing process (Salmi et al., 2016). However, parameters such as the occupied build area and other manufacturing process parameters are relevant to measuring manufacturing process time (Zhang et al., 2015). Additionally, manufacturing process parameters, such as layer thickness, affect the achievable manufacturing time (Kretzschmar et al., 2018; Flores et al., 2020).

Table 2 shows the vector of design variables (Xd2) used to model the manufacturing process time (Mt). In this regard, height (H), build area (A), and the average material ratio of $\overline{Vf}$ were modified in a three-level DOE. The subsystem optimisation objective for the manufacturing discipline (i.e., J2) is to minimise the manufacturing time (Mt).
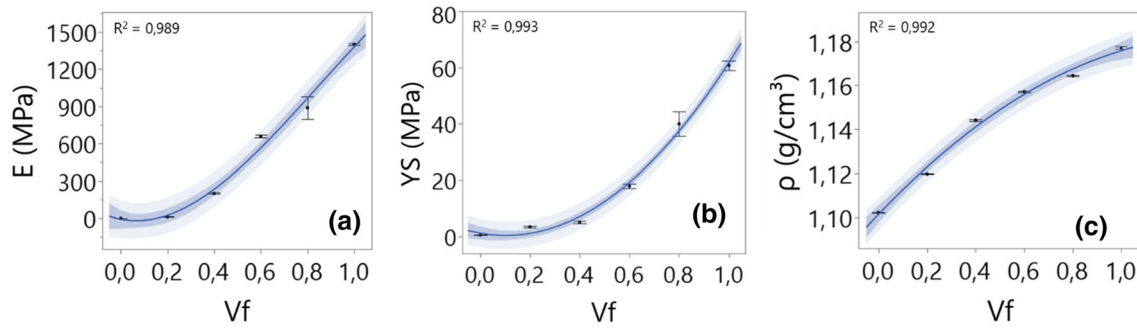
Fig. 5 Regression model for material homogenization based Vf microstructural descriptor. **a** Cubic regression model of Young's modulus (E). **b** Quadratic regression model of yield strength (YS). **c** Quadratic regression model of density (ρ)

Table 2 DOE for the manufacturing subsystem discipline (D2)

Design variables (Xd2)	Nomenclature	Levels
Height	H (cm)	2–10–18
Build area	A (cm^2)	582–1170–1728
Average volume fraction	$\overline{Vf}$	0–0.5–1

The manufacturing time was estimated using GrabCad print (Stratasys, 2022), a software pre-processor that simulates manufacturing time while connected to the Stratasys J750 material jetting AM system. The printing mode recorded was at high-mix with a layer thickness of 0.27 mm, the same manufacturing process parameter used to fabricate the tensile specimens in the material discipline (D1). The manufacturing time was estimated using different rectangular parallelograms modelled as "stl" files, uploaded to the GrabCad print pre-processing software to simulate each DOE combination proposed in Table 2.

The build volume of the material jetting J750 machine defines the lower and upper bounds for height and build area. During the DOE, the height (H) of the rectangular parallelogram was varied in three discrete intervals of 2 cm, 10 cm, and 18 cm, respectively. Thus, the section or projected area (A) of the parallelograms was varied in three discrete intervals of 582 cm^2, 1170 cm^2, and 1728 cm^2, respectively, such that the area represents 30%, 60%, and 90% occupation of the build platform, respectively. Ultimately, the material impact in process time was modelled by changing the Vf in three levels as 0.0, 0.5, and 1.0, which represent the average use of volume fraction between Vero and Tango ($\overline{Vf}$) in the design. In total, this DOE recorded 27 test trials with no need for repetition due to the deterministic nature of the pre-processing software.

The results of the DOE were analysed using an ANOVA test with a confidence level of 95% ($\alpha = 0.05$). Mt is modelled using response surface approximating functions with second-order polynomial two-factor interactions terms described in

Eq. (3):

$$y = \beta_o + \sum_{i=1}^{k} \beta_i x_i + \sum_{i=1}^{k} \beta_{ii} x_i^2 + \sum_i \sum_j \beta_{ij} x_i x_j + \varepsilon \quad (3)$$

where ε is the unobserved random error, β represent the coefficients of the regression model for each term (i.e. intercept β_o, first-order β_i, second-order β_{ii}, and the interaction term β_{ij}) calculated by the least square method, x_i represent the independent variables H, A, and Vf. The interaction terms between independent variables are represented by $x_i x_j$ and y is the dependent manufacturing time (Mt).

Similar to the material subsystem modelling, a stepwise regression was used to eliminate non-significant terms, and the stopping rule was set with a forward P-value < 0.25. Appendix 1 presents the regression results for Mt as a function of H, A, and Vf. Figure 6a shows the contour plot for H and A over Mt. In this regard, the colour map from dark to light corresponds to achievable manufacturing time (Mt). The horizontal axis of the contour plot corresponds to part build area (A) and the vertical axis represents part height (H).

Figure 6b shows the factor plot of the effect of the independent variables on the response manufacturing time (Mt). The part orientation in the build platform was simplified by running the part location function in the GrabCad print pre-processing software, which optimizes the build orientation to minimize the height and reduce manufacturing time. The factor plot also includes the effect of varying material volume fraction (Vf) on Mt. The factor plots show the confidence interval at 95%, representing a range of likely values for the mean response.

As a principle, the more significant the difference between the mean effect's minimum and maximum value, the higher its significance and, therefore, the influence of the independent variable over the response. By comparing the mean effect of H, A, and Vf, over the response Mt, part height (H) is the most significant variable followed by surface area (A), which significantly affects the Mt. On the contrary, Vf has a limited effect on MT. Nevertheless, the ANOVA test shows
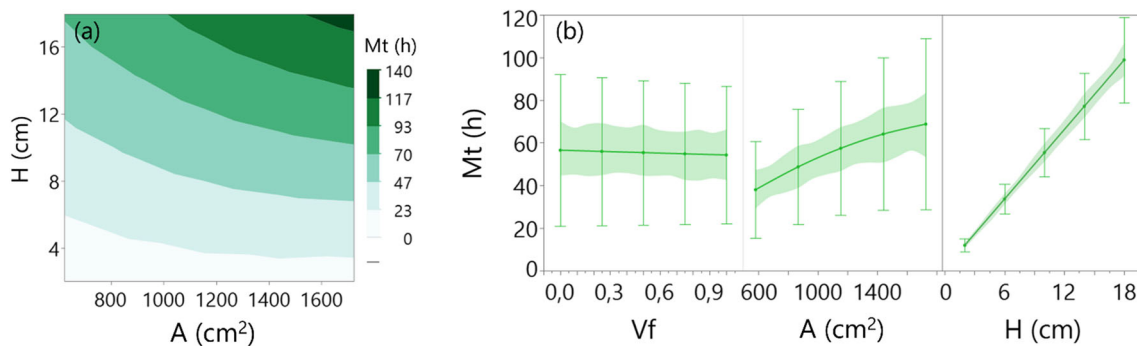
Fig. 6 **a** Contour plot of the effect of H and A on Mt. **b** Factor plot on the effect of H, A, and Vf on manufacturing time (Mt)

Table 3 DOE for the product-design subsystem discipline (D3)

Design variable (Xd3)	Nomenclature	Levels
Rigid region thickness	Rt (mm)	5–10–15–20–25
Material—rigid region	Vf_{Rigid}	0,4–0,6–0,8–1
Soft region thickness	St (mm)	6
Material—soft region	Vf_{Soft}	0

that the interaction effect between H and Vf (i.e., $H*Vf$) has reduced the p-value (i.e., P-value = 0.129). Therefore, it significantly impacts the response and is included as a term in the regression model. Looking at the first-order terms, the increase of Vf harms Mt. On the contrary, the interaction term $H*Vf$ has a positive effect on Mt.

Product-design discipline

The Product-design subsystem is studied using FEA model-based approach, where an elastic isotropic material model was assumed. The socket design, depicted in Fig. 2, is composed of two regions. The region in contact with the skin is soft with silicone like behaviour and a rigid region responsible for providing the required stiffness to make the prosthetic functional. For this study, the product-design discipline (D3) was explored by maintaining a constant thickness and material properties at the soft region (St), whereas the design space of the rigid region was explored by varying the thickness (Rt) and the mechanical properties (i.e., E, YS, and ρ as a function of Vf). In the case of the soft region, St was set to 6 mm and the material characteristic of the soft region was set to $Vf_{Soft} = 0$, which provides elastic properties similar to silicone with a Young's modulus of 0.53 ± 0.04 MPa, elongation at break of 94.94 ± 3.68 mm, and a yield strength 0.47 ± 0.02 MPa. In the case of the rigid region, the socket design requires a stiffer material for structural integrity; hence the design space exploration was limited to $0.4 \leq Vf_{Rigid} \leq 1$. Table 3 shows the design variables (Xd3) and bounds used to model the product-design discipline (D3).

For the design space exploration of D3, we included two dependent variables: safety factor (Sf), which is used to define the constraint function in the MDO, and maximum total deformation (D), which becomes an optimisation objective. The Sf was evaluated by looking at the resulting maximum von Mises stress of the FEA socket design. The von Mises yield criterion states that the von Mises stress of a material under load must be less than or equal to the yield strength of the material under simple tension for the resulting design to be able to withstand the loading conditions. The Sf allowed determining if a given combination of Vf and Rt will yield or fracture, thus, resulting in a mechanically non-feasible socket design. The Eq. (4) is used to construct the constraint function, defined by the margin of safety (Sf) described as:

$$Sf = (Yield\ Strength/Max.von\ Mises\ stress)_i - 1 \quad (4)$$

where the subscript i represents the experimental combinations of the DOE, supposing that the resulting Sf is equal to 0, the maximum von Mises stress and yield strength are equal, hence capable of withstanding the loads and boundary conditions. If the Sf < 0, the resulting socket design is under-engineered, and it would yield or fracture, resulting in a non-feasible solution, whereas an Sf > 0 represents that the socket design is over-engineered.

The resulting values of the FEA provide the maximum value of deformation of the socket per experimental combination. Maximum Deformation (D) is calculated by the square root of the summation of the square of maximum deformations in X-direction, Y-direction, and Z-direction. During the design of the prosthetic, controlling D provides the possibility to vary the overall stiffness and flexibility of the socket design, which can be leveraged and tailored based on user preferences. Figure 7 shows the contour plot of the feasible design space with Rt and Vf as a function of the margin of safety (Sf), which is the inequality constraint function. The FEA, and the resulting polynomial model, shows that certain combinations of Vf and Rt would provide negative values for
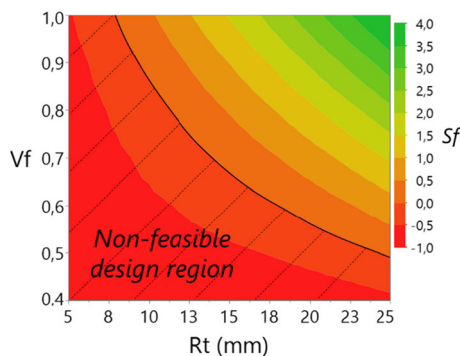
Fig. 7 Contour plot based on the polynomial RSM. Effect of *Rt* and *Vf* on safety factor (Sf)

Sf. This region provides non-feasible solutions as the resulting socket design would yield or fracture.

During the design engineering of the socket, the decision-maker can decide between three optimisation alternatives for the subsystem optimisation objective (J3): (i) Minimization of D to obtain the stiffest socket design (i.e., scenario 1 for optimisation), which advanced prosthetic users and professional athletes can use. (ii) Maximization of D to obtain the softest available design (i.e., scenario 2 for optimisation) to increase the comfort of early users of prosthetic sockets. Additionally, an inductive design approach can be taken (Choi et al., 2008). Hence, (iii) the stiffness level and deformation (D) can be set to a target value based on patient preferences (i.e., scenario 3 for optimisation). The MDO would provide Vf and Rt values that lead to an optimal set of feasible and non-dominated solutions (J*).

System-level MDO problem formulation

In this MDO problem formulation, material discipline is coupled with product design (i.e., D1–D3), as the variation in *Vf* affects the mechanical properties (i.e., E and YS), and therefore the constraint function margin of safety (Sf) and disciplinary design optimisation objective (J3) that is total deformation (D). Product-design to manufacturing (i.e., D3–D2) is coupled by the variation of $\overline{Vf}$ which has an impact on the manufacturing time (Mt). More significantly, the variation of the thickness of the rigid region of the prosthetic (*Rt*) affects part height (*H*) and projected area (*A*), and therefore the manufacturing time (Mt). Similarly, design choices in product design are coupled with material and resulting part mass (i.e., D3–D1). To this end, the variation of *Rt* affects the obtained volume of the prosthetic socket, and the variation of *Vf* affects part density. The resulting product-design combinations for *Vf* and *Rt* determine the product volume, material density, and product mass. The resulting subsystem disciplinary surrogate models are summarized in Appendix 1. Table 4 shows the formalized MDO problem for-

Table 4 MDO problem formulation for the prosthetic socket design

Given

The optimisation objectives, constraint functions, variables, and coupling function shared between material discipline D1, manufacturing discipline D2, and product-design discipline D3 (see Appendix)

Find

Subsystem level variables: *Vf* and *Rt*

Satisfy

Product-design (D3) subsystem level constraint function:

Inequality constraint:

$Sf \geq 0$

Equality constraint (soft region):

$St(mm) = 6$

$Vf_{Soft} = 0$

Goals (objective functions):

(J1) Min {mass (gr)}: part weight

(J2) Min {time (h)}: manufacturing time

(J3) Max, min, and on target {D (mm)}: total deformation

Bounds

Material subsystem D1 (Xd1):

$0 \leq Vf \leq 1$

Manufacturing subsystem D2 (Xd2):

$0 \leq A(cm^2) \leq 1911$

$0 \leq H(cm) \leq 20$

$0 \leq \overline{Vf} \leq 1$

Product-design D3 (Xd3):

Rigid region:

$5 \leq Rt(mm) \leq 25$

$0.4 \leq Vf \leq 1$

System-level optimisation objective (J*):

An optimal set of feasible and non-dominated solutions

mulation for the presented case study of a prosthetic socket design produced by material jetting AM.

MDO solution methods for design space exploration and exploitation

Embodiment design using a Bayesian network

Bayesian networks (BN) are an effective tool for decision making and reasoning under uncertainty. Their popularity has risen in the last decade due to their ability to handle incomplete datasets by encoding statistical dependencies between the variables, ability to explore causal relationships between the variables within a system and to model domain knowledge and data simultaneously, making them a sophisticated package for data analysis (Heckerman et al., 1995).

In the context of complex manufacturing process modelling, BN support decision making through reasoning and integrated product-process models can be created to explore regions of interest in the design space during embodiment stages of design (James et al., 2012; Shahan & Seepersad, 2012; Wu & Wang, 2021). In comparison to function-oriented methods, BN modelling is progressive. BN allows integration of data or functional models at any stage of the model development and, therefore, is especially suitable at the embodiment design stage (Hou & Jiao, 2020). BNs enable the combination of multidisciplinary models, expert knowledge, and data by providing a global and intuitive view of dependencies (Moullec et al., 2013). Embodiment design and exploration can be facilitated by defining statistical distributions of the design vector variables, and the likelihood of the optimisation objectives can be calculated using the Bayesian theorem. The likelihood of the objective gives the information about what area (or range) of the design variables has a higher probability of generating expected designs (Nannapaneni et al., 2017).

We used BayesiaLab 8 for the development and simulation of the BN model. At its core, a BN presents a modular and efficient representation of the joint probability distribution of a set of domain variables. The Bayes theorem powers the inference mechanism in a BN wherein the probability of occurrence of an event can be estimated based on prior knowledge of conditional relation to the event (mathematical expression presented in Appendix 2). A BN can be constructed to represent the dependencies within a system comprising of all variables and decisions. The variables or decisions are represented by nodes connected by arcs to signify conditional probability dependence, while the absence of an arc signifies conditional independence. Parent nodes feed dependencies into the dependent child nodes, forming a hierarchy of decisions.

Based on the dependencies between different variables, the joint probability distribution (JPD) of a BN can be factorized into a set of conditional probability tables at the nodes given their parent nodes. By manipulating the JPD of the network with a large number of variables can be time-consuming, local computations of posterior probabilities in the presence of new information using conditional independence assumptions of the variables modelled, speeding up the inference mechanism (Lauritzen & Spiegelhalter, 1988; McNaught & Chan, 2011). The BN uses the conditional and marginal probability tables at each node to make inferences during simulations (Koller et al., 2007). The development of the BN for embodiment design for the MDO problem formulation is explained below.

To produce a BN in the context of this research, we created a directed acyclic graph (DAG) (Iwasaki & Simon, 1994). The graph in Fig. 8 is represented as a colour-coded DAG depicting the PSPP linkages for the prosthetic device. The
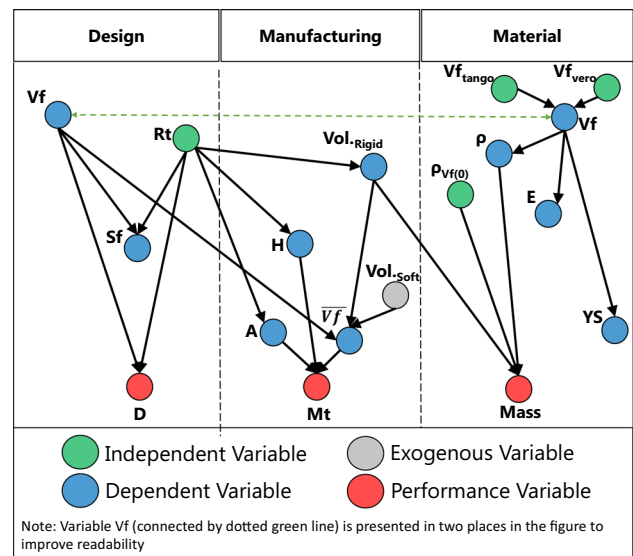

Fig. 8 Colour coded directed acyclic graph system model of an AM prosthetic socket design

DAG is constructed based on the set of equations and the associated ranges of values described in Appendix 1. The probabilistic relations modelled in the BN for the case study are shown in Appendix 2. The parent nodes or independent variables (represented in green) within the developed network consisting of four nodes (Rt, Vf_{Tango}, Vf_{Vero}, $\rho_{Vf(0)}$) are assigned a prior marginal probability distribution (MPD) of the form $P(Node) \sim U(a, b)$ which represents a uniform probability distribution between a and b. The domain of each parent node is split into a number of states of equal range. The parent nodes feed dependencies into the child nodes (9 child nodes, represented in blue).

The relationship between the parent nodes and child nodes is modelled using the surrogate models presented in Appendix 1. Based on the relationship, the domain of the variable (child nodes) is calculated and assigned to equal states within the node. Conditional probability tables (CPT) are then computed within the network for the child nodes, given the probability of their respective parent nodes. Finally, the target nodes (Mass, Mt, and D) are performance variables in the system model represented in red. The target nodes are child nodes for which conditional probability tables are computed like other child nodes. The mathematical expression for computation of the conditional probability distribution in the child nodes follows the Bayes theorem shown in Appendix 2.

In addition, equality and inequality constraint nodes (4) are added between nodes (Vf, Sf), (Vf, mass), (Vf, Mt) and (Vf, D) to ensure that the value of Vf remains between 0.4 and 1 following the MDO problem constraint. Thus, conditional probability values for the states of the variable Vf < 0.4 are set to be zero. This implies that any values of mass,

Mt, D, and Sf when Vf is less than 0.4 are not considered in the network computations during simulation. The JPD of the BN is calculated using the equation shown in Appendix 2 to compute the probability of all possible events in the network as defined by the combination of the values of all the variables. However, the BN factors the joint distribution into conditional distributions of variables locally, given the parent nodes of the variable. In addition, the independence assertion that each variable is only dependent on its immediate parents helps speed up the computation. Thus, during the simulation of a fully specified BN, the posterior probabilities of any subset of variables are computed bidirectionally, given evidence about another variable subset using the Bayes theorem.

For this specific problem formulation, the BN is used to harness the variation of design variables (i.e., Xdi) and map the feasible design space. Besides, we wanted to identify the region of interest that optimizes the objective functions while satisfying the constraint functions. A BN allowed us to characterise the effect of design variables on the target variables and map the region of interest leading to optimal results. The BN can be expanded to include expert product knowledge to determine variable constraints and uncertainties and ascertain variable interrelationships. Besides, the BN can guide a resampling strategy to be implemented at the detail design. Thus, adding data points can increase the local accuracy of the models for the exploitation phase (Xiong et al., 2019).

Based on the inequality constraint on the safety factor, the design space is classified into two regions, feasible and non-feasible (i.e., feasible if Sf ≥ 0). The obtained feasible region still comprises a multitude of design solutions. To further narrow down the solution space, the BN explores optimal regions of the design space and reduces solution space to probabilistically optimal solutions. The Bayesian inference is built on top of the developed DAG. The BN comprises 21 nodes, 17 for variables and 4 for constraints (shown in Appendix 2), with each node divided into states. Each variable in the DAG is designed as a node with multiple states within the BN, such that the range of values the variable can take is equally distributed based on the number of states defined for that specific node. The nodes are connected with the help of directed arrows whose direction determines the parent–child relationship between the nodes. The independent variables in this study are defined using a uniform distribution divided into n number of states. The probability of the variable to take a value within any of its defined states is equal at the independent nodes. The range of values for dependent nodes is based on the node connections coming into the node. Thus, the probability of each state of a dependent variable is calculated based on the conditional probability tables generated for the dependent nodes (child nodes).

Once all the nodes and their connections are defined, the BN model can be simulated for variables of interest by providing evidence to the nodes of the network. It is important to note that the underlying mechanism for developing the DAG and hence, the BN is modular and is dependent on the variable interactions represented as equations. Designers can simulate and assess the three subsystems collectively and independently. For specific levels of granularity warranted, designers can redefine or update system boundaries, add or remove the connections and nodes, and changes can be made to their states and value range within each node. In this research, more states are provided for nodes Rt and Vf than others to aid in the design of space exploration.

Detailed design using desirability functions and Pareto Front

The detailed design requires that all three objective functions need to be optimized concurrently. In this specific MDO problem formulation, the objective functions were modelled using response surface approximating functions with second-order polynomial two-factor interactions terms. The response surface optimisation and desirability function approach introduced by Derringer and Such (1980) was implemented where the optimisation objectives of each were simulated to isolate the Pareto Frontier (PF) of non-dominated solutions such that no design solution can improve one criterion without diminishing at least another criterion. The resulting PF contains all dominant solutions with a maximum overall desirability score.

Desirability function-based methods transforms the estimated response models ($\hat{y}$), into individual desirability functions (d) that are then aggregated into a composite function (Des.). This function is usually a geometric or an arithmetic mean, which will be maximized or minimized, respectively (Costa et al., 2011). Derringer and Such proposed individual desirability functions based on three response types as follows: Nominal-The-Best (NTB) (i.e., scenario 3 for optimisation—obtain target deformation socket design), where the value of the estimated response is expected to achieve–a particular target value (T). For this response type, the individual desirability function is defined as:

$$d = \begin{cases} \left(\frac{\hat{y}-L}{T-L}\right)^S, & L \leq \hat{y} \leq T \\ \left(\frac{\hat{y}-L}{T-U}\right)^t, & L \leq \hat{y} \leq T \\ 0, & otherwise \end{cases} \quad (5)$$

where S are t are user-specified parameters ($S, t > 0$) thast allow the system designer to specify the shape of d. The individual desirability function transforms the response variable into a range of values between 0 and 1, where 1 is most favorable. In the NTB case, $d = 1$ for $\hat{y} = T$, and $d = 0$ for $\hat{y} < L$ or for $\hat{y} > U$, where U is the upper and L is the lower specification limit of the response.

Larger-The-Best (LTB) (i.e., scenario 2 for optimisation—obtain the softest socket design), where the value of the estimated response is expected to be larger than a lower bound ($\widehat{y} > L$). For this response type, the individual desirability function is defined as:

$$d = \left(\frac{\widehat{y} - L}{U - L}\right)^r, \; L \leq \widehat{y} \leq U \qquad (6)$$

where r is a user-specified parameter ($r > 0$). In the LTB case one assumes that it is possible to establish a finite target U such that $d = 1$ for $\widehat{y} \geq U$ and $d = 0$ for $\widehat{y} \leq L$.

Smaller-The-Best (STB) (i.e., scenario 1 for optimisation—obtain the stiffest socket design), where the value of the estimated response is expected to be smaller than an upper bound ($\widehat{y} < U$). For this response type, the individual desirability function is defined as:

$$d = \left(\frac{\widehat{y} - U}{L - U}\right)^r, \; L \leq \widehat{y} \leq U \qquad (7)$$

under the assumption that it is possible to establish a finite target L such that $d = 1$ for $\widehat{y} > L$, and $d = 0$ for $\widehat{y} \geq U$.

The values assigned to s, t, and r allow changing the shape of d. Illustrative plots for different weights and discussion on their choice are presented by Kros and Mastrangelo (2004). The basic idea of the desirability function approach is to transform a multi-response problem into a single response problem transforming it mathematically. To simultaneously optimize several responses, each of these disciplinary desirability scores is combined using the geometric mean that leads to the overall desirability score for each design solution. In essence, this transformation condenses a multivariate optimisation problem into a univariate one, with the ability to compare the overall desirability score as a function of one or more independent variables. Mathematically speaking, Eq. (8) defines the overall desirability score as:

$$Des. = (d_1 * d_2 * d_3 * \ldots * d_n)^{1/n} \qquad (8)$$

where (Des.) represents the overall desirability score that is calculated by the geometric mean of individual d_n, which represents each individual transformed response of the objective functions (i.e., J1—Mass, J2—Manufacturing time, and J3—Total deformation). The rationale behind using the geometric mean is that if any quality characteristic has an undesirable value (i.e., $d_n = 0$) at a particular region of the combination of design variables, the overall result is a product that will return an unacceptable solution (Derringer & Suich, 1980).

The simulation and optimisation during the exploitation phase are based on a gradient descent algorithm as the design variables are continuous. The gradient-based optimisation algorithm is used to find the values of a function's parameters (coefficients) that minimize a cost function as far as possible (Burke et al., 2018). The choice of desirability functions and weighting factor depends on the priorities of the decision-maker. This allows integrating prior knowledge or preferences. The transformed response d_i obtains a value 0 when the outcome represents a completely undesirable response and obtains value of 1 for the most desirable response (Fuller & Scherer, 1998). In transforming objective functions to desirability scores, the sensitivity allocation of "preferences" per design scenario was considered in the analysis of optimal design solutions.

Results: prosthetic socket design

Embodiment design and solution space exploration

The BN is simulated to optimize the disciplinary objectives in two scenarios. Scenario 1: (i) minimizing both mass (J1) and manufacturing time (J2), along with minimizing the total deformation (J3) of the product to obtain the stiffest socket design. Scenario 2: (ii) minimizing both the mass (J1) and manufacturing time (J2) while maximizing the total deformation (J3) to obtain the most flexible design. Figure 9 shows the BN design space exploration results, including results prior to optimisation and scenarios 1 and 2. In Fig. 9, the target or performance variables of the model (optimisation objective in the context of MDO) is represented in (a), the dependent variable (safety constraint in MDO) is presented in (b), and the independent variables of the model are presented in (c).

The BN model is simulated backwards to perform the exploration study for the different scenarios. It is important to note that a forward simulation could also be executed to perform predictive analysis moving from independent variables to the targets. Prior to optimisation, the left-most column in Fig. 9 represents the default probability values for the states of the performance and design variables (i.e., mass, Mt, D, Vf, Rt, and Sf). The probability for Vf < 0.4 is set to zero to satisfy the product design inequality constraint, as shown in Table 4. The simulation output provides equal probabilities for states of independent variables and conditional probabilities for states of dependent variables when no evidence is provided to the BN. It is observed that only 35.73% of solutions in the design space satisfy the safety constraint for the current configuration of the BN (see prior to optimisation in Fig. 9). The probabilities for all states of node Rt are observed to be 5% each.

Optimal solutions need to be feasible, and therefore, they must satisfy the inequality constraint such that Sf ≥ 0. For scenario 1, hard evidence was provided to nodes mass, Mt, and D to optimise (i.e., stiffest socket design while minimizing Mt and mass). The probability of the three nodes was set to be 100% at the lowest possible state of each node. Scenario
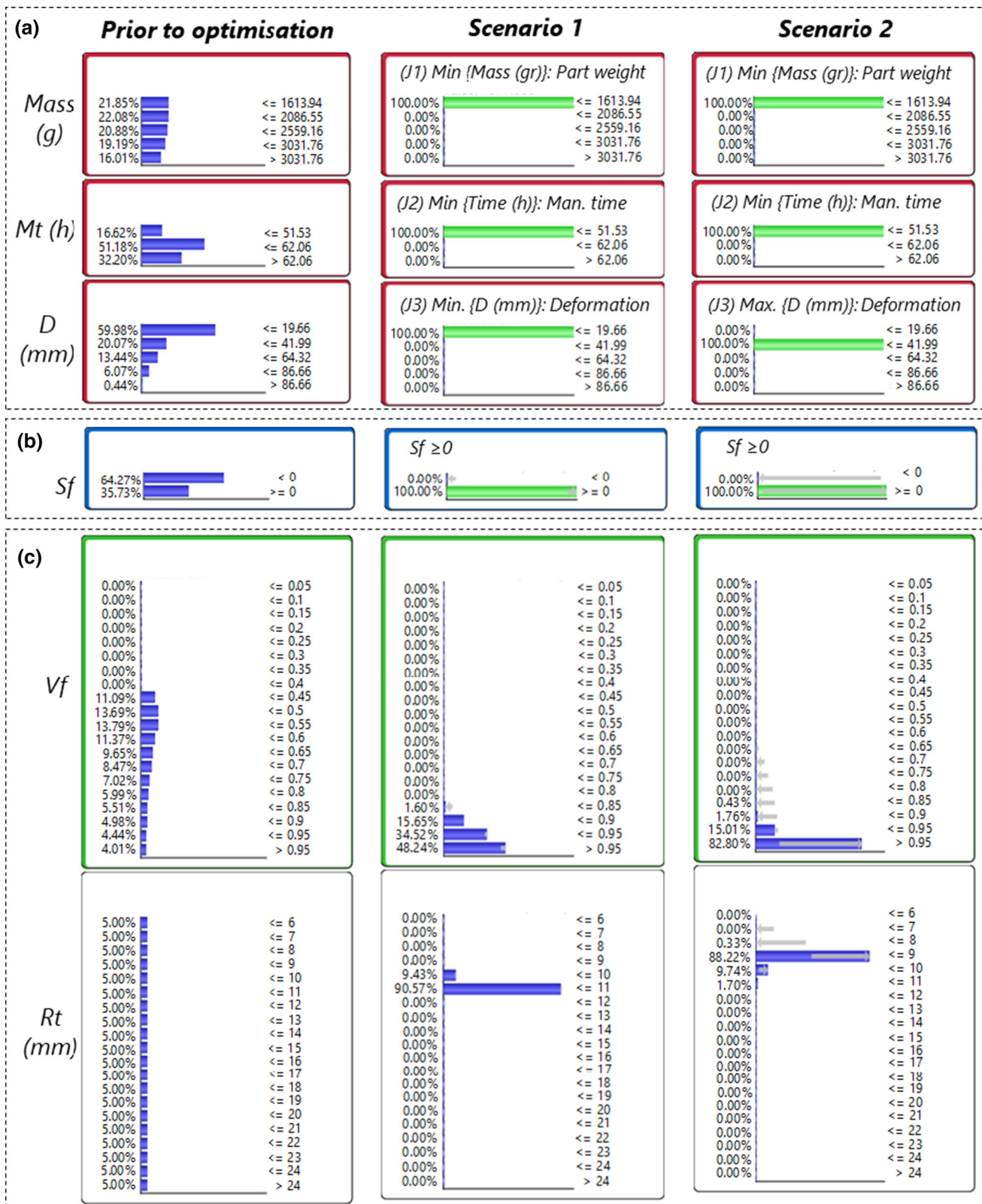
Fig. 9 BN design space exploration (**a** erformance variables, **b** dependent variable, **c** Independent variables) prior to optimisation for scenario 1 and scenario 2
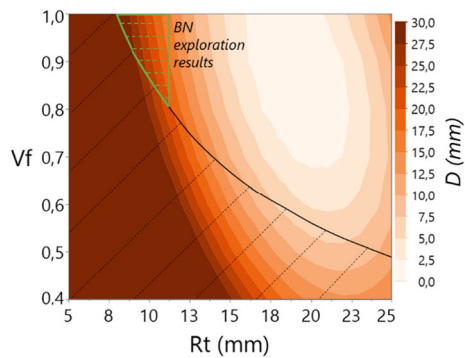
Fig. 10 Contour plot on the effect of *Rt* and *Vf* on total deformation (D) and overlay view of the non-feasible design region and BN exploration results

1 results show the effect of these choices on nodes Rt and Vf. Vf at a state where its value is greater than 0.95 has the highest probability (48.24%). Overall, several design solutions exist for 0.85 < Vf ≤ 1. Similarly, for Rt, the highest probability of 90.57% was observed for 10 < Rt ≤ 11 and overall, design solutions exist for 9 < Rt ≤ 11.

For scenario 2 (i.e., most flexible socket design while minimizing Mt and mass), hard evidence of 100% probability was provided to nodes mass and Mt to lie in their lowest possible states. Upon setting the evidence for mass and Mt, it was observed that the probability of states for node D was zero for any value of D > 41.99. Thus, to maximize J3, hard evidence of 100% probability was applied to the state in which the highest possible value of D was present, thus 19.66 < D ≤ 41.99. Scenario 2 simulation shows the effect of these choices on nodes Rt and Vf. The highest probability was observed for Vf > 0.95 at 82.80%, and design solutions exist for 0.85 < Vf ≤ 1. Similarly, for Rt, the highest probability of 88.22% was observed for 9 < Rt ≤ 10, and design solutions exist for 7 < Rt ≤ 11. Figure 10 shows the resulting contour plot of *Rt* and *Vf* as a function of the total deformation (D). Results show a strong preference for a stiff material, even if high deformation is desired.

The contour plot displays the overlaid view of the non-feasible design region, thus failing to satisfy the constraint of Sf ≥ 0. The contour also combines the results obtained from the BN exploration scenarios, defining a narrower design space for the detail design stage. The observation results from the BN simulations provide the region that leads to optimal outcomes for both scenarios and can define a resampling plan for additional FEA simulations to increase local accuracy at the detail design and exploitation phase (Xiong et al., 2019).

Detailed design and solution space exploitation

Figure 11 shows the design alternatives' impact on predictions for D, Mt, and mass simultaneously. The design space shows the combinations of *Rt* and *Vf* that lead to feasible and
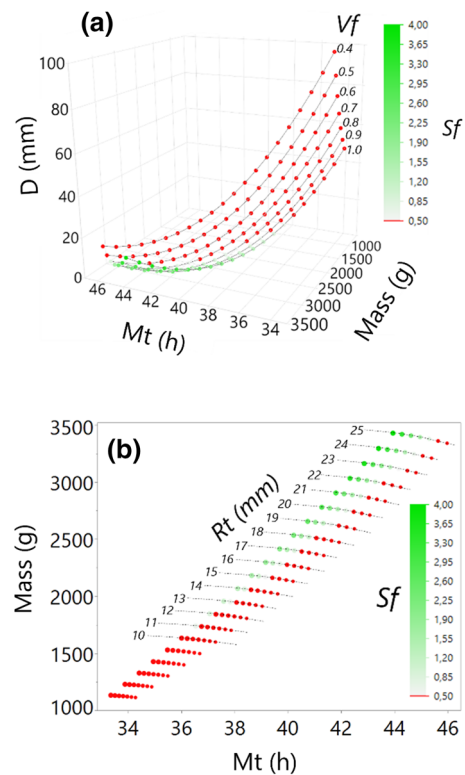

Fig. 11 Design space results, including feasible and non-feasible solutions. **a** 3D scatterplot for D as a function of mass, Mt, and resulting Sf. **b** 2D scatter plot for mass as a function of Mt and resulting Sf

non-feasible solutions. In Fig. 11 (a), the surface plot shows how increasing *Vf* values to *Vf* ≥ 0.6 lead to solutions that satisfy Sf ≥ 0.5. On the other hand, Fig. 11b shows the scatter plot of Sf as a function of mass and MT. In this case, results for *Rt* ≥ 12 mm led to a solution that satisfies Sf ≥ 0.5. In the exploitation phase, a more restrictive Sf constraint is used for the design exploitation phase, representing solutions that lead to product design disciplinary alternatives with Sf ≥ 0.5 and resulting in solutions where yield strength is at least 1.5 times the Von Mises stress (these solutions are coloured in green, and therefore feasible).

The results of design "preferences" for the design exploitation phase are provided in Table 5. We present a comparison of design scenarios where optimisation objectives and design constraints are modified, simulating different design preferences. All the simulated design scenarios consider the objectives to minimize socket Mt and mass. Comparing scenario 1 (i.e., minimization of D to obtain the stiffest socket design) design preferences, maximization of the Sf constraint (i.e., scenario 1.0) and a solution where Sf is fixed to 0.5 (i.e., scenario 1.1). Maximizing Sf leads to the stiffest solution for the socket (i.e., D = 1.32 mm) at the cost of providing the highest Mt and mass for the socket (i.e., Mt = 39.76 h and mass = 2426.89 g). On the other hand, targeting a Sf = 0.5 leads to an increased deformation (i.e., D = 5.95 mm), while

Table 5 Design scenarios to minimize socket Mt and mass, considering different optimisation objectives for D, and Sf constraints

Scenario No	Opt. objective (D) and design constraint (Sf)	Rt (mm)	Vf	D (mm)	Mt (h)	Mass (g)	Sf	Des
1.0	Min. {D (mm)}; while Max. {Sf ≥ 0.5}	17.09	1	1.32	39.76	2426.89	2.05	0.58
1.1	Min. {D (mm)}; while Target {Sf = 0.5}	15.53	0.77	5.95	39.52	2228.58	0.50	0.68
2.0	Max. {D (mm)}; while Max. {Sf ≥ 0.5}	11.85	1	13.08	36.99	1830.27	0.82	0.51
2.1	Max. {D (mm)}; while Target {Sf = 0.5}	10.37	1	19.27	36.20	1671.29	0.50	0.90
3.0	Target {D (mm) = 8}; while Max. {Sf ≥ 0.5}	13.39	1	8.00	37.80	1999.67	1.16	0.58
3.1	Target {D (mm) = 8}; while Target {Sf = 0.5}	13.12	0.96	8.00	37.58	1986.48	0.5	0.73

improving Mt and mass (i.e., Mt = 39.52 h and mass = 2228.58 g) and overall desirability score (i.e., Des. = 0.68).

The design preferences in scenario 2 (i.e., maximization of D to obtain the softest available design) between maximization of the Sf constraint (i.e., scenario 2.0) and a solution where Sf is fixed to 0.5 (i.e., scenario 2.1) lead to a different design outcome. Maximizing Sf leads to a more conservative deflection (i.e., D = 13.08 mm) and increased Mt and mass for the socket (i.e., Mt = 36.99 h and mass = 1830.27 g). In comparison, targeting a Sf = 0.5 leads to the highest possible deformation (i.e., D = 19.27 mm), while improving Mt and mass (i.e., Mt = 36.20 h and mass = 1671.29 g) and highest overall desirability score (i.e., Des. = 0.90).

Ultimately, scenario 3 (i.e., target deformation value based on patient preferences) compares design preferences in terms of Sf when deformation is set to a middle value (i.e., D = 8 mm). Maximizing Sf (i.e., scenario 3.0) leads and increased Mt and mass for the socket (i.e., Mt = 37.80 h and mass = 1999.67 g) in comparison to a solution where Sf is fixed to 0.5 (i.e., scenario 3.1) that provide slightly more reduced Mt and mass for the socket design (i.e., Mt = 37.58 h and mass = 1986.48 g) and higher overall desirability score (i.e., Des. = 0.73).

To summarize the results of Table 5, the relative difference of mass from the stiffest to softest designs presented in Table 5 provides a variation of 31.13%, corresponding to a considerable reduction of mass of 755.6 g from the heaviest and stiffest design to the lightest and softest design. Manufacturing time (Mt) is less affected and provide optimal solutions with an 8.95% difference from stiffest to softest design. Defining the design Sf constraint impacts the resulting design alternative significantly. For example, selecting a more conservative design with a higher Sf led to a lowering overall desirability score, hence results that tend to be heavier and have a longer manufacturing time. On the other hand, reducing the Sf and targeting an Sf = 0.5 (i.e., solutions where yield strength is 1.5 times the Von Mises stress) increases the desirability score, leading to lighter designs and faster manufacturing.

Figure 12 shows how the design exploitation phase can be presented graphically. Figure 12a shows a 3D scatterplot for D as a function of mass and Mt. This figure shows a Monte-Carlo simulation of 4500 design alternatives that minimize mass and Mt, while satisfying Sf ≥ 0.5. The Pareto Front (PF) is isolated and represented by red point markers. In contrast, blue point markers represent dominated solutions.

Figure 12b shows a 2D scatter plot for D as a function of mass, and the resulting Rt is represented in a colour gradient. The following Fig. 12c zooms into the PF and shows all the design scenarios to minimize socket Mt and mass, considering different optimisation objectives for D and different Sf constraints as presented in Table 5. Four out of six design preferences presented in Table 5 are non-dominated solutions. However, design preferences that imposed a Sf = 0.5 lead to theoretical dominated solutions (i.e., S1.1 and S3.1).

Conclusions and future work

Enhancing the intelligence of manufacturing systems requires that material systems, design engineering, and manufacturing systems are better connected. New computer expert systems must support our ability to explore and exploit cause-effect and interrelationships across disciplines more efficiently, thus expanding the human cognitive capabilities.

This research has connected a material micro-scale descriptor (Vf) and product design choices (Rt) into a broader MDO problem formulation that includes multiple system-level disciplinary optimisation objectives of a prosthetic socket product design. The initial exploration was assisted at the embodiment design with probabilistic reasoning based on a Bayesian network (BN). The detail design stage showed how to optimise all three objective functions using a desirability function approach and gradient descent optimisation algorithm to isolate non-dominated solutions. The resulting problem formulation is used to generate feasible solutions representing the best trade-off in the Pareto Front (PF) that

Fig. 12 Pareto Front (PF) and design space exploitation of feasible solutions. **a** 3D scatterplot for D as a mass function, and Mt shows the PF and dominated solutions. **b** 2D scatter plot for D as a function of mass and resulting Rt and Vf. **c** 2D scatter plot for D as a function of mass and resulting Sf showing the PF results and design preferences
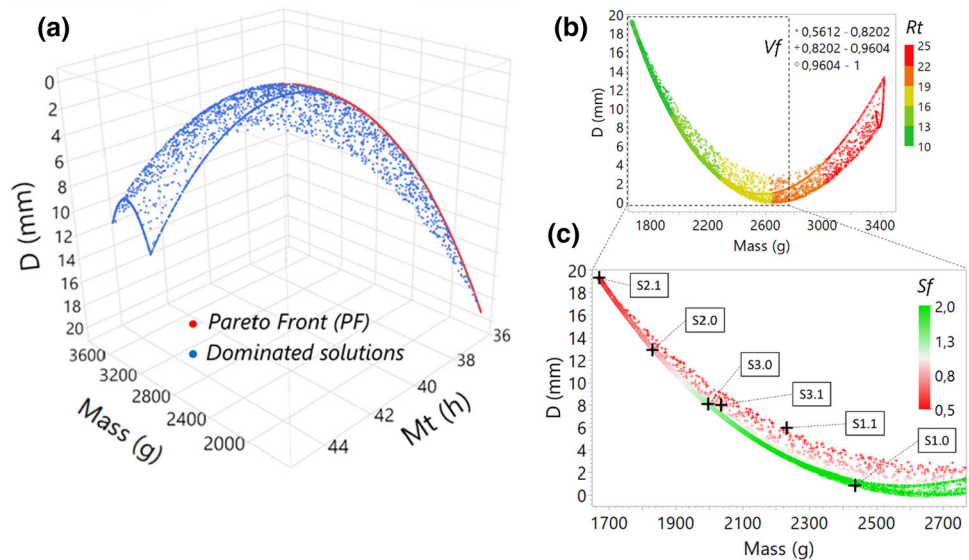
satisfy disciplinary constraints and optimise objective functions during the product design of an exemplary prosthetic socket. The primary contribution and novelty of this research are:

- To combine data-driven and model-based analysis methods to create multi-fidelity surrogate models in an exploration and exploitation problem formulation using a prosthetic socket design as a case study.
- To develop an optimisation-driven design methodological approach to be generalisable and adaptable to a large variety of engineering design problems.
- To demonstrate how engineering decisions at the material micro-scale (i.e., Vf) and product design choices (i.e., Rt) had a ripple effect on concurrent disciplines across length scales. Product performance was mathematically intertwined with manufacturing, material systems, and engineering design choices to increase system designers' cognitive ability to find optimal solutions.
- To conceptualise a computer-aided expert system capable of exploring process-structure–property-performance (PSPP) linkages in a digital manufacturing process.

Future research is planned to develop a higher-fidelity FEA model capable of more reliably describing a socket design's behaviour and extending the problem formulation to include a larger vector of design variables. For example, we plan (i) problem formulations, including surrogate modelling selection and validation methods for higher dimensionality problems. This was limited intentionally to simplify the problem and interpretability of the socket study case. Besides, we plan to include (ii) more disciplinary interactions as coupling functions as represented by the dotted lines in Fig. 3 (e.g., variation of manufacturing process variables and its effect on material structure D2–D1), (iii) other material systems, including metallic materials and interactions with process and heat-treatments, and (iv) considering different sources of uncertainty from material system models, to manufacturing and engineering design.

This socket study case was limited and cannot be used in a real application context. To this end, considerable effort is required to bring this specific design problem to a real-world application, necessitating higher-fidelity mechanical FEA simulations, functional prototyping, and validation test studies involving prosthetists and patients. Nevertheless, prosthetic sockets and similar applications can be engineered using multidisciplinary exploration and exploitation strategies. Hence, balancing stiffness and lightweight design while combining multi-materials properties creates rigid and soft pads in the socket's specific "pain" areas. Besides, an inductive design approach is highly desirable for end-users. Hypothetically, the level of stiffness and deformation (D) can be predefined at different socket regions. During the product design, PSPP variables will be adjusted to provide optimal solutions that tailor performance in an integrated digital manufacturing and design workflow to produce "one-of-a-kind" prosthetics that are anatomically customised and mechanically engineered to consider patient preferences and comfort.

In summary, optimisation-driven design poses significant challenges. The design space must be defined and intertwined mathematically in a problem that is neither entirely understood nor necessarily appreciated across disciplines. One could imagine the next generation of novel multi-scale computer-aided systems capable of exploring

and exploiting the linkages at process, structure, property, and performance levels tailoring the system to be capable of solving specific product-design needs. Potentially, material and manufacturing multi-fidelity models and advanced design synthesis methods can be interlinked with advanced computer-aided systems that consider product-design variables and expected performance. That being said, similar exploration and exploitation approaches can be extended to more diverse and sophisticated problem formulations dictated by a particular application, manufacturing processes, and material systems.

It can be argued that the entire design discipline is "problem-centred". On the other hand, once the material system and manufacturing disciplines are modelled, they can support all kinds of design problems. For example, if a new design problem emerges, the material and manufacturing surrogates can be "called" within the computer expert system to assist in decision-making. Thus, providing the system designer with the necessary information to drive the design process considering the ripple effects of design choices in material and manufacturing disciplines. The ongoing research effort is focused on modelling other material, manufacturing, and design processes involving machine learning and artificial neural networks. Thus, allowing engineering designers the holistic exploration and exploitation using computer-aided systems tailored explicitly for intertwined digital manufacturing and design processes.

Author Contributions IFI developed the main conceptual ideas, planned the research, conducted the experiments, built the models and simulations, prepared the artwork, and wrote the manuscript. SP contributed to the methodology by integrating the Bayesian network to explore the design space at the embodiment design stages, HPNN worked on developing the graph-based model adapted into a directed acyclic graph for the development of the Bayesian network. HPNN and SP contributed to writing and reviewing the manuscript contributing significantly to its completion. DWR and EC contributed to the conceptual ideas and reviewed the manuscript. All authors contributed to the concepts, methodology, and results, reviewed the manuscript and contributed to its finalisation.

Declarations

Appendix 1

Equs.	Functions	MDO framework	Summary of Fit	
(9)	$E(MPa) =$ $-7976 - 372,073Vf + 2895,553Vf^2 - 1134,028Vf^3$ Where; $0 \leq Vf \leq 1$	D1–D3	RSquare	0.989009
			RSquare Adj	0.986654
			RMSE	60.71065
			Mean	527.1156
			Observations	18
(10)	$YS(MPa) = 1143 - 15,753Vf + 76,332Vf^2$ Where; $0 \leq Vf \leq 1$	D1–D3	RSquare	0.992673
			RSquare Adj	0.991696
			RMSE	2.075053
			Mean	21.25444
			Observations	18
(11)	$A(cm^2) = 365.671 + 9.726Rt - 0.273Rt^2 + 0.005Rt^3$ Where; $5 \leq Rt(mm) \leq 25$	D3–D2	RSquare	0.999886
			RSquare Adj	0.999544
			RMSE	0.91435
			Mean	465.12
			Observations	5
(12)	$H(cm) = 14,130 + 0,193Rt$ Where; $5 \leq Rt(mm) \leq 25$	D3–D2	RSquare	0.999681
			RSquare Adj	0.999575
			RMSE	0.031623
			Mean	17.04
			Observations	5
(13)	$\overline{Vf} = [(Vol._{Soft}/Vol._{Total}) * Vf_{Soft}] +$ $[(Vol._{Rigid}/Vol._{Total}) * Vf]/2$ Satisfy; $Vol._{Soft} = 490,9cm^3$ (8.1) $Vf_{Soft} = 0$ (8.2) Where; $0 \leq \overline{Vf} \leq 1$	D3–D2		
(14)	$Vol._{Rigid}(cm^3) = 166.2 + 73,642Rt + 0.740Rt^2 + 0.002Rt^3$ Where; $5 \leq Rt(mm) \leq 25$	D3–D1	RSquare	1
			RSquare Adj	1
			RMSE	0.119523
			Mean	1487
			Observations	5
(15)	$Sf = 1653 - 0249Rt - 5.58Vf + 0.00285Rt^2 + 2543Vf^2 +$ $0401Rt * Vf$ Satisfy; $Sf \geq 0$ Where; $5 \leq Rt(mm) \leq 25$ $0.4 \leq Vf \leq 1$	D3 (Constraint function)	RSquare	0.995716
			RSquare Adj	0.993931
			RMSE	0.113362
			Mean	0.492167
			Observations	18

Equs.	Functions	MDO framework	Summary of Fit	
(16)	$D(mm) = 218, 291 - 14, 258Rt - 191, 744Vf + 0.2866Rt^2 + 68, 597Vf^2 + 3714Rt * Vf$ Where; $5 \leq Rt(mm) \leq 25$ $0.4 \leq Vf \leq 1$	J3	RSquare	0.883631
			RSquare Adj	0.835143
			RMSE	8.361109
			Mean	18.32945
			Observations	18
(17)	$Mt(h) = -15, 911 + 2714H + 0.029A + 4130\overline{Vf} - 0.000012A^2 + 0.002628H * A - 0.637H * \overline{Vf}$ Where; $0 \leq A(cm^2) \leq 1911$ $0 \leq H(cm) \leq 20$ $0 \leq \overline{Vf} \leq 1$	J2 (Min.)	RSquare	0.98484
			RSquare Adj	0.980292
			RMSE	5.573067
			Mean	54.90259
			Observations	27
(18)	$\rho(g/cm^3) = 1.101 + 0.116Vf - 0.041Vf^2$ $mass(g) = (Vol._{Rigid} * \rho_{Vf(i)}) + (Vol._{Soft} * \rho_{Vf(0)})$ Where; $0.4 \leq Vf \leq 1$ Satisfy; $Vol._{Soft} = 490.9cm^3$ $\rho_{Vf(0)} = 1.119 \pm 0.061g/cm^3$	J1 (Min.)	RSquare	0.991623
			RSquare Adj	0.989762
			RMSE	0.002735
			Mean	1.1441
			Observations	12

Appendix 2

Legend
- Parent Node
- Constants
- Child Node
- Target

Bayes Theorem

$$P(A|B) = \frac{P(B|A).P(A)}{P(B)}$$

Where A and B represents two events, whose independent probabilities are P(A) and P(B) respectively. P(A|B) and P(B|A) are conditional probabilities of event A and event B occurring.

Joint Probability Distribution (JPD)

$$P(U) = \prod_i P(V_i | pa(V_i))$$

Where $P(U)$ is the joint probability of the network, $pa(V_i)$ is the set of parents of variable V_i

Prior Marginal Probability Distributions (4 Nodes)

- Rt — $P(Rt) \sim U(5,25)$
- Vf_{tango} — $P(Rt) \sim U(0,1)$
- Vf_{vero} — $P(Rt) \sim U(0,1)$
- $\rho_{Vf(0)}$ — $P(Rt) \sim U(1.058,1.18)$

Conditional Probability Distributions (9 Nodes)

- Vf — $P(Vf | Vf_{tango}, Vf_{vero})$
- Sf — $P(Sf | Rt, Vf)$ Appendix A, Eq. 15
- H — $P(H | Rt)$ Appendix A, Eq. 12
- A — $P(A | Rt)$ Appendix A, Eq. 11
- ρ — $P(\rho | Vf)$ Appendix A, Eq. 18
- E — $P(E | Vf)$ Appendix A, Eq. 9
- YS — $P(YS | Vf)$ Appendix A, Eq. 10
- Vol_{Rigid} — $P(Vol_{Rigid} | Rt)$ Appendix A, Eq. 14
- $\overline{Vf}$ — $P(\overline{Vf} | Vol_{Rigid}, Vf)$ Appendix A, Eq. 13

Constants (1 Node)
- Vol_{Soft} — Value = 490.9

Constraints
- $0.4 \leq Vf \leq 1$

Targets (3 Nodes)

- D — $P(D | Rt, Vf)$ Appendix A, Eq. 16
- Mt — $P(Mt | H, A, \overline{Vf})$ Appendix A, Eq. 17
- Mass — $P(Mass | Vol_{Rigid}, \rho)$ Appendix A, Eq. 18

References

Balling, R. J., & Sobieszczanski-Sobieski, J. (1996). Optimization of coupled systems—A critical overview of approaches. *AIAA Journal, 34*(1), 6–17. https://doi.org/10.2514/3.13015

Ballardini, R. M., Flores Ituarte, I., & Pei, E. (2018). Printing spare parts through additive manufacturing: Legal and digital business challenges. *Journal of Manufacturing Technology Management, 29*(6), 958–982. https://doi.org/10.1108/MRR-09-2015-0216

Bass, L., Meisel, N. A., & Williams, C. B. (2016). Exploring variability of orientation and aging effects in material properties of multi-material jetting parts. *Rapid Prototyping Journal, 22*(5), 826–834. https://doi.org/10.1108/RPJ-11-2015-0169

Burke, S. E., Anderson-Cook, C. M., Lu, L., & Montgomery, D. C. (2018). Prioritization of stockpile maintenance with layered Pareto fronts. *Quality Engineering, 30*(4), 556–568. https://doi.org/10.1080/08982112.2017.1390585

Choi, H.-J., Allen, J. K., Rosen, D., McDowell, D. L., & Mistree, F. (2008). An Inductive Design Exploration Method for the Integrated Design of Multi-Scale Materials and Products. https://doi.org/10.1115/DETC2005-85335

Coello, C. A. C. (1999). A comprehensive survey of evolutionary-based multiobjective optimization techniques. *Knowledge and Information Systems, 1*(3), 269–308. https://doi.org/10.1007/BF03325101

Comotti, C., Regazzoni, D., Rizzi, C., & Vitali, A. (2017). Pressure data and multi-material approach to design prosthesis. In H. M. Fardoun, V. M. R. Penichet, D. M. Alghazzawi, & M. E. De la Guia (Eds.), *ICTs for improving patients rehabilitation research techniques* (pp. 35–45). Springer. https://doi.org/10.1007/978-3-319-69694-2_4

Conner, B. P., Manogharan, G. P., Martof, A. N., Rodomsky, L. M., Rodomsky, C. M., Jordan, D. C., & Limperos, J. W. (2014). Making sense of 3-D printing: Creating a map of additive manufacturing products and services. *Additive Manufacturing, 1–4*, 64–76. https://doi.org/10.1016/j.addma.2014.08.005

Costa, N. R., Lourenço, J., & Pereira, Z. L. (2011). Desirability function approach: A review and performance evaluation in adverse conditions. *Chemometrics and Intelligent Laboratory Systems, 107*(2), 234–244. https://doi.org/10.1016/j.chemolab.2011.04.004

Derringer, G., & Suich, R. (1980). Simultaneous optimization of several response variables. *Journal of Quality Technology, 12*(4), 214–219. https://doi.org/10.1080/00224065.1980.11980968

Faustini, M. C., Neptune, R. R., Crawford, R. H., Rogers, W. E., & Bosker, G. (2006). An experimental and theoretical framework for manufacturing prosthetic sockets for transtibial amputees. *IEEE Transactions on Neural Systems and Rehabilitation Engineering, 14*(3), 304–310. https://doi.org/10.1109/TNSRE.2006.881570

Ferguson, S., Kasprzak, E., & Lewis, K. (2009). Designing a family of reconfigurable vehicles using multilevel multidisciplinary design optimization. *Structural and Multidisciplinary Optimization, 39*(2), 171–186. https://doi.org/10.1007/s00158-008-0319-3

Foort, J. (1965). The patellar-tendon-bearing prosthesis for below-knee amputees, a review of technique and criteria. *Artificial Limbs, 9*(1), 4–13.

Flores Ituarte, I., Boddeti, N., Hassani, V., Dunn, M. L., & Rosen, D. W. (2019). Design and additive manufacture of functionally graded structures based on digital materials. *Additive Manufacturing, 30*, 100839. https://doi.org/10.1016/j.addma.2019.100839

Flores, I., Kretzschmar, N., Azman, A. H., Chekurov, S., Pedersen, D. B., & Chaudhuri, A. (2020). Implications of lattice structures on economics and productivity of metal powder bed fusion. *Additive Manufacturing, 31*, 100947. https://doi.org/10.1016/j.addma.2019.100947

Fuller, D., & Scherer, W. (1998). The desirability function: Underlying assumptions and application implications. In *SMC'98 Conference Proceedings. 1998 IEEE International Conference on Systems, Man, and Cybernetics (Cat. No.98CH36218), 4*, 4016–4021 (Vol. 4). https://doi.org/10.1109/ICSMC.1998.726717

Ghiabakloo, H., Lee, K., Kazeminezhad, M., & Kang, B. S. (2016). Surrogate-based Pareto optimization of annealing parameters for severely deformed steel. *Materials & Design, 92*, 1062–1069. https://doi.org/10.1016/j.matdes.2015.11.059

Hachisuka, K., Dozono, K., Ogata, H., Ohmine, S., Shitama, H., & Shinkoda, K. (1998). Total surface bearing below-knee prosthesis: Advantages, disadvantages, and clinical implications. *Archives of Physical Medicine and Rehabilitation, 79*(7), 783–789. https://doi.org/10.1016/S0003-9993(98)90356-2

Hashemi, S. M., Parvizi, S., Baghbanijavid, H., Tan, A. T. L., Nematollahi, M., Ramazani, A., Fang, N. X., & Elahinia, M. (2022). Computational modelling of process–structure–property–performance relationships in metal additive manufacturing: A review. *International Materials Reviews, 67*(1), 1–46. https://doi.org/10.1080/09506608.2020.1868889

Heckerman, D., Geiger, D., & Chickering, D. M. (1995). Learning Bayesian networks: The combination of knowledge and statsitical data. *Machine Learning, 20*, 197.

Hou, L., & Jiao, R. J. (2020). Data-informed inverse design by product usage information: A review, framework and outlook. *Journal of Intelligent Manufacturing, 31*(3), 529–552. https://doi.org/10.1007/s10845-019-01463-2

Iwasaki, Y., & Simon, H. A. (1994). Causality and model abstraction. *Artificial Intelligence, 67*(1), 143–194. https://doi.org/10.1016/0004-3702(94)90014-0

James, T. P., Pearlman, J. J., & Saigal, A. (2012). Rounded cutting edge model for the prediction of bone sawing forces. *Journal of Biomechanical Engineering*. https://doi.org/10.1115/1.4006972

Jiang, J., Xiong, Y., Zhang, Z., & Rosen, D. W. (2022). Machine learning integrated design for additive manufacturing. *Journal of Intelligent Manufacturing, 33*(4), 1073–1086. https://doi.org/10.1007/s10845-020-01715-6

Kodiyalam, S., & Sobieszczanski-Sobieski, J. (2001). Multidisciplinary design optimization-some formal methods, framework requirements, and application to vehicle design. *International Journal of Vehicle Design, 25*(1–2), 3–22.

Koller, D., Friedman, N., Džeroski, S., Sutton, C., McCallum, A., Pfeffer, A., Abbeel, P., Wong, M.-F., Meek, C., & Neville, J. (2007). *Introduction to statistical relational learning*. MIT press.

Kretzschmar, N., Flores Ituarte, I., & Partanen, J. (2018). A decision support system for the validation of metal powder bed-based additive manufacturing applications. *The International Journal of Advanced Manufacturing Technology, 96*(9), 3679–3690. https://doi.org/10.1007/s00170-018-1676-8

Kros, J. F., & Mastrangelo, C. M. (2004). Comparing multi-response design methods with mixed responses. *Quality and Reliability Engineering International, 20*(5), 527–539. https://doi.org/10.1002/qre.664

Laszczak, P., Jiang, L., Bader, D. L., Moser, D., & Zahedi, S. (2015). Development and validation of a 3D-printed interfacial stress sensor for prosthetic applications. *Medical Engineering & Physics, 37*(1), 132–137. https://doi.org/10.1016/j.medengphy.2014.10.002

Lauritzen, S. L., & Spiegelhalter, D. J. (1988). Local computations with probabilities on graphical structures and their application to expert systems. *Journal of the Royal Statistical Society Series B (methodological), 50*(2), 157–224.

Mak, A., Zhang, M., & Boone, D. A. (2001). State-of-the-art research in lower-limb prosthetic biomechanics. *Journal of Rehabilitation Research and Development, 38*, 161–174.

Martins, J. R. R. A., & Lambe, A. B. (2013). Multidisciplinary design optimization: A survey of architectures. *AIAA Journal, 51*(9), 2049–2075. https://doi.org/10.2514/1.J051895

McNaught, K., & Chan, A. (2011). Bayesian networks in manufacturing. *Journal of Manufacturing Technology Management, 22*(6), 734–747. https://doi.org/10.1108/17410381111149611

Meng, D., Li, Y., He, C., Guo, J., Lv, Z., & Wu, P. (2021). Multidisciplinary design for structural integrity using a collaborative optimization method based on adaptive surrogate modelling. *Materials & Design, 206*, 109789. https://doi.org/10.1016/j.matdes.2021.109789

Miao, B. R., Luo, Y. X., Peng, Q. M., Qiu, Y. Z., Chen, H., & Yang, Z. K. (2020). Multidisciplinary design optimization of lightweight carbody for fatigue assessment. *Materials & Design, 194*, 108910. https://doi.org/10.1016/j.matdes.2020.108910

Moullec, M.-L., Bouissou, M., Jankovic, M., Bocquet, J.-C., Réquillard, F., Maas, O., & Forgeot, O. (2013). Toward system architecture generation and performances assessment under uncertainty using Bayesian networks. *Journal of Mechanical Design*. https://doi.org/10.1115/1.4023514

Mueller, J., Shea, K., & Daraio, C. (2015). Mechanical properties of parts fabricated with inkjet 3D printing through efficient experimental design. *Materials & Design, 86*, 902–912. https://doi.org/10.1016/j.matdes.2015.07.129

Nannapaneni, S., Liang, C., & Mahadevan, S. (2017). Bayesian network approach to multidisciplinary, multi-objective design optimization under uncertainty. In *18th AIAA/ISSMO Multidisciplinary Analysis and Optimization Conference*. American Institute of Aeronautics and Astronautics. https://doi.org/10.2514/6.2017-3825

Nti, I. K., Adekoya, A. F., Weyori, B. A., & Nyarko-Boateng, O. (2022). Applications of artificial intelligence in engineering and manufacturing: A systematic review. *Journal of Intelligent Manufacturing, 33*(6), 1581–1601. https://doi.org/10.1007/s10845-021-01771-6

Olson, G. B. (1997). Computational design of hierarchically structured materials. *Science, 277*(5330), 1237–1242. https://doi.org/10.1126/science.277.5330.1237

Oztemel, E., & Gursev, S. (2020). Literature review of Industry 4.0 and related technologies. *Journal of Intelligent Manufacturing, 31*(1), 127–182. https://doi.org/10.1007/s10845-018-1433-8

Pahl, G., Beitz, W., Feldhusen, J., & Grote, K. (2007). *Engineering design: A systematic approach* (3rd ed., p. 632). Springer.

Panchal, J. H., Choi, H.-J., Shephard, J., Allen, J. K., McDowell, D. L., & Mistree, F. (2008). A strategy for simulation-based multiscale. *Multi-Functional Products and Associated Design Processes*. https://doi.org/10.1115/DETC2005-85316

Riesenfeld, R. F., Haimes, R., & Cohen, E. (2015). Initiating a CAD renaissance: Multidisciplinary analysis driven design: Framework for a new generation of advanced computational design, engineering and manufacturing environments. *Computer Methods in Applied Mechanics and Engineering, 284*, 1054–1072. https://doi.org/10.1016/j.cma.2014.11.024

Rogers, B., Stephens, S., Gitter, A., Bosker, G., & Crawford, R. (2000). Double-wall, transtibial prosthetic socket fabricated using selective laser sintering: A case study. *JPO Journal of Prosthetics and Orthotics, 12*(3), 97–103.

Rosen, D. W. (2014). Research supporting principles for design for additive manufacturing. *Virtual and Physical Prototyping, 9*(4), 225–232. https://doi.org/10.1080/17452759.2014.951530

Ryu, J. E., Salcedo, E., Lee, H. J., Jang, S. J., Jang, E. Y., Yassi, H. A., Baek, D., Choi, D., & Lee, E. (2019). Material models and finite analysis of additively printed polymer composites. *Journal of Composite Materials, 53*(3), 361–371. https://doi.org/10.1177/0021998318785672

Salmi, M., Flores Ituarte, I., Chekurov, S., & Huotilainen, E. (2016). Effect of build orientation in 3D printing production for material extrusion, material jetting, binder jetting, sheet object lamination, vat photopolymerisation, and powder bed fusion. *International Journal of Collaborative Enterprise*. https://doi.org/10.1504/IJCENT.2016.10003187

Sanders, J. (2005). Stump-socket interface conditions. In D. L. Bader, C. V. C. Bouten, D. Colin, & C. W. J. Oomens (Eds.), *Pressure ulcer research: Current and future perspectives* (pp. 129–147). Springer. https://doi.org/10.1007/3-540-28804-X_9

Sato, S., Togo, N., & Yamanaka, S. (2016). Designing functional beauty through additive manufacturing: Prototyping of running specific prostheses using selective laser sintering. In *2016 International Solid Freeform Fabrication Symposium*. Retrieved September 11, 2022 from https://hdl.handle.net/2152/89712

Serhat, G., & Basdogan, I. (2019). Multi-objective optimization of composite plates using lamination parameters. *Materials & Design, 180*, 107904. https://doi.org/10.1016/j.matdes.2019.107904

Shahan, D. W., & Seepersad, C. C. (2012). Bayesian network classifiers for set-based collaborative design. *Journal of Mechanical Design*. https://doi.org/10.1115/1.4006323

Simpson, T., Toropov, V., Balabanov, V., & Viana, F. (2008). Design and analysis of computer experiments in multidisciplinary design optimization: A review of how far we have come—or not. In *12th AIAA/ISSMO Multidisciplinary Analysis and Optimization Conference*. American Institute of Aeronautics and Astronautics. https://doi.org/10.2514/6.2008-5802

Smith, J., Xiong, W., Yan, W., Lin, S., Cheng, P., Kafka, O. L., Wagner, G. J., Cao, J., & Liu, W. K. (2016). Linking process, structure, property, and performance for metal-based additive manufacturing: Computational approaches with experimental support. *Computational Mechanics, 57*(4), 583–610. https://doi.org/10.1007/s00466-015-1240-4

Stratasys. (2022). *Stratasys direct: Manufactured parts on demand*. Retrieved September 11, 2022 from https://www.stratasys.com/en/stratasysdirect/

Wang, G. G., & Shan, S. (2006). Review of metamodeling techniques in support of engineering design optimization. *Journal of Mechanical Design, 129*(4), 370–380. https://doi.org/10.1115/1.2429697

Wu, D., & Wang, G. G. (2021). Causal artificial neural network and its applications in engineering design. *Engineering Applications of Artificial Intelligence, 97*, 104089. https://doi.org/10.1016/j.engappai.2020.104089

Xiong, Y., Duong, P. L. T., Wang, D., Park, S.-I., Ge, Q., Raghavan, N., & Rosen, D. W. (2019). Data-driven design space exploration and exploitation for design for additive manufacturing. *Journal of Mechanical Design*. https://doi.org/10.1115/1.4043587

Xiong, Y., Tang, Y., Park, S.-I., & Rosen, D. W. (2020). Harnessing process variables in additive manufacturing for design using manufacturing elements. *Journal of Mechanical Design*. https://doi.org/10.1115/1.4046069

Yan, W., Lian, Y., Yu, C., Kafka, O. L., Liu, Z., Liu, W. K., & Wagner, G. J. (2018a). An integrated process–structure–property modeling framework for additive manufacturing. *Computer Methods in Applied Mechanics and Engineering, 339*, 184–204. https://doi.org/10.1016/j.cma.2018.05.004

Yan, W., Lin, S., Kafka, O. L., Lian, Y., Yu, C., Liu, Z., Yan, J., Wolff, S., Wu, H., Ndip-Agbor, E., Mozaffar, M., Ehmann, K., Cao, J., Wagner, G. J., & Liu, W. K. (2018b). Data-driven multi-scale multi-physics models to derive process–structure–property relationships for additive manufacturing. *Computational Mechanics, 61*(5), 521–541. https://doi.org/10.1007/s00466-018-1539-z

Zhang, Y., Bernard, A., Valenzuela, J. M., & Karunakaran, K. P. (2015). Fast adaptive modeling method for build time estimation in Additive Manufacturing. *CIRP Journal of Manufacturing Science and Technology, 10*, 49–60. https://doi.org/10.1016/j.cirpj.2015.05.003

Zhong, R. Y., Xu, X., Klotz, E., & Newman, S. T. (2017). Intelligent manufacturing in the context of industry 4.0: A review. *Engineering, 3*(5), 616–630. https://doi.org/10.1016/J.ENG.2017.05.015